
LOCKHEED

MISSILES & SPACE COMPANY, INC. • SUNNYVALE, CALIFORNIA

CONTENTS

## ILLUSTRATIONS



## TABLES

## ABSTRACT

Lockheed Missiles & Space Company (LMSC) has been developing, on Independent Development (ID) funds, a Structural Alignment Sensor (SAS) for use with large deployable antenna systems for contour measurement and/or active control. The SAS is a laser ranging system using frequency modulation and accurate phase measurement to determine distance. Initially, work was done with a $CO_2$ laser. This work has been extended to the use of a HeNe laser. LMSC contracted with Jet Propulsion Laboratory (JPL) to demonstrate the capability of the SAS to measure antenna rib contours over ranges of 50 meters to a resolution of 100 $\mu$m.

Initial resolution data was taken with the $CO_2$ system. This data shows that it will indeed meet the SAS requirements. Shortly after the initiation of this contract, LMSC began the development of the HeNe system which is attractive because it offers substantial improvement in size, weight, and power over the $CO_2$ system. The final demonstration was made with the HeNe system and it too showed that the SAS requirements could be met with this alternate approach.

This report projects these results to a conceptual design for a flight system and describes how it might be used.

## NEW TECHNOLOGY

No new technology was developed under this contract. All the technology applied was developed under LMSC Independent Development funds and is reported in LMSC IR&D Reports for 1977/78 and 1978/79.

# 1.0 SUMMARY

## 1.1 INTRODUCTION

The need for a non-contact measurement system to assist with the development and deployment of large antennas has been evident for a number of years. In 1977, under company Independent Development (ID) funds, Lockheed Missiles & Space Company (LMSC) undertook the development of a Structural Alignment Sensor (SAS).

The SAS system used a frequency modulated $CO_2$ laser with heterodyne detection and a unique phase measurement scheme. The phase measurements were then converted to distance. Analytical predictions and preliminary test results showed that this system would be capable of measuring distance over ranges of 50 meters with an accuracy of 100 $\mu$m. LMSC proposed to the Jet Propulsion Laboratory (JPL) that, upon the completion of a breadboard system at LMSC in 1978, a demonstration would be prepared which would show the capability of the SAS to measure antenna contours with the above range and resolution.

## 1.2 PROGRAM DEVELOPMENT

About the time the contractual effort began, the LMSC ID program was redirected to study the use of a HeNe laser instead of a $CO_2$ laser. A HeNe laser would offer the advantages of much smaller components, smaller power requirements, non-cryogenic detectors, and visual alignment.

An analytical study was performed which showed that when retro-reflectors are used over the specified range, the HeNe system should actually outperform the $CO_2$ system. Where very large ranges or specular reflection returns from unprepared surfaces are used, the higher power of the $CO_2$ laser gives it the advantage. Since both systems used the same operating frequencies, the signal processing electronics could be common. The HeNe system was breadboarded and a demonstration performed.

## 1.3 TEST RESULTS

Prior to implementation of the HeNe system, resolution data was taken with the $CO_2$ system with results well within the 100 $\mu$m goal. There was some apparent skewing of the wavefront across the beam, making the distance measurement very sensitive to beam direction; therefore, neither multi-target nor long path tests were performed. The cause of this problem was a wavefront skew from the Bragg cell, and a solution is being worked on.

The HeNe system also had some development difficulty associated with laser stability. For proper operation, a highly stable, single-mode laser is required. This was not obtainable in the time period of the contract so a partially successful attempt was made to modify an unstable, multimode laboratory laser for this purpose. Nevertheless the laser remained stable for short periods during which good data was obtained. The resolution goal was demonstrated and a long-path test performed. To minimize external influences such as vibration and atmosphere, a multi-folded path was used. This caused a large reflection loss (44 bounces) reducing the signal-to-noise ratio by 20 db. A corresponding increase in sensor noise was observed; otherwise the system performed satisfactorily. In addition, the resolution could be demonstrated only when the target alone was being measured. Measuring both target and reference, as the final system will do, caused an increase in noise by a factor of three. This is most likely caused by optical feedback due to the instability of the laser used and should be resolved early in the 1979 ID effort.

## 1.4 PROJECTED FLIGHT SYSTEM

The analysis and test results show the feasibility of developing a system for space flight application. To meet the accuracy of 100 $\mu$m, up to 10 targets per second could be sampled with an external beam directing system. The SAS itself would occupy about 0.15 cubic meters, weigh 10 kilograms and consume 400 watts of prime source. With the HeNe system, inexpensive glass retro-reflectors could be used. The development costs, for such a system including a prototype, have been estimated to be about $1.5 M, with additional units costing about $0.5 M each.

# 2.0 THEORY OF OPERATION

## 2.1 INTRODUCTION

The SAS measures distance by accurately measuring phase of a modulated laser beam. Distance to a reference point is compared with the distance to the target. This method eliminates, through common moding, any drifts prior to the output beam-splitter. Actual implementation of the $CO_2$ and HeNe systems differed optically; this is discussed in Section 3. The following discussion applies to both systems.

An optical layout of the SAS is illustrated in Figure 1. The beam from the laser is both spatially and frequency shifted by the Bragg cell. The unshifted portion of the beam is used as the local oscillator for the heterodyne receiver. The shifted beam is directed through the phase modulator with mode matching lenses. This modulated beam is split, and one sent to the reference mirror and the other to the target. Two choppers, $180^{o}$ out of phase, sample the beams alternately for signal processing. For the demonstration, a mirror on a rotary table was used to direct the beam to the targets. Both the reference beam and target beam are returned to combine with the local oscillator beam to be received by the detector.

The processing electronics consist of the system described in Section 3, as well as a micro-processor for converting the signals to a digital range output. From the micro-processor output and the rotary table position, the rib contour can be calculated.

## 2.2 UNIQUE SIGNAL PROCESSING CONCEPT

LMSC has breadboarded the signal processing scheme described in this section and demonstrated its performance. Theoretical derivations for the signal processor are provided in Section 2.3. All referenced equations are to be found in that section.

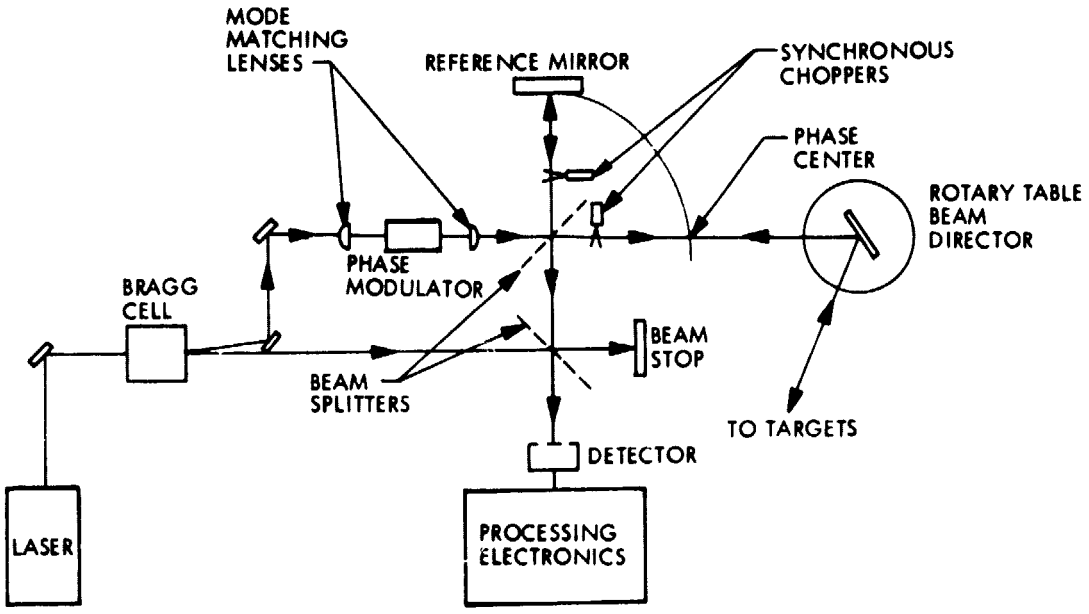


Fig. 1 SAS Optical Layout Diagram

The laser source is either the $CO_2$ or HeNe laser. The laser beam passes successively through two Bragg cells providing a doubly offset frequency which is the "working" laser beam. That beam which is not frequency displaced in the first Bragg cell is used as the local oscillator beam. Use of the double Bragg cells provides effective isolation of the laser from any perturbation due to returned working beam power. This is so because of the combination of doubled frequency offset and power attenuation of any working beam power able to retrace its path into the laser. The use of Bragg cells thus provides the multiple advantages of (1) providing a frequency offset which permits optical heterodyne detection, (2) permitting selection of the offset (or subsequent IF) frequency at some optimum value, and (3) preserving laser stability by effective isolation from any returned working beam power.

The processing flow is shown in Figure 2. Beginning in the upper left-hand corner, FM modulation frequencies of 1.0 or 100 MHz are selectable by the RF switch. The selected RF power is divided and the first fraction passes successively through an adjustable (phase shifting) transmission line, a power amplifier, and a phase modulator for the working beam. This portion of the circuit provides the phase modulation, $\phi(m)$, shown in Section 2.3. The other fraction of the RF power passes to the $90^{o}$ hybrid where about one-half the power is phase shifted and two outputs corresponding to sine and cosine functions are provided. These outputs, each with a phase and amplitude trimmer, go to the inputs of a pair of SPST RF switches. The switch output provides the following RF mixer with sine and cosine inputs on alternate half cycles. Its output after the following bandpass filter corresponds to the right sides of Equations (9) and (10). The crystal detector, amplifier, and logarithmic voltmeter provide the output shown in Equation (12).

Observe in Figure 2, that phase shifting is used to move the observation close to a phase angle of $45^{o}$ or $45^{o} \pm N \times 90^{o}$. The phase shifting can be accomplished by several methods and the switching of calibrated delay lines is a case in point. Whatever technique is used requires that the phase shift calibration and stability be compatible with the range resolution required. For the case of switched delay lines used as an example, this applies to both delay lines and the switches.

Observation of delay line and switch stability have been made for the 100 MHz amplitude modulation case. The stability has been found compatible with the range resolution requirements discussed above. Additional support for this conclusion is provided by the results of range resolution measurements described in Section 2.3.3.

## 2.3 SIGNAL PROCESSING THEORY

Photomixing the optical local oscillator and target-sensing beams produces signal components (two sidebands) consisting of a mix between the dual Bragg cell-generated acoustic frequency and the electro-optic modulator phase modulation frequency (carrying range information) of the following form:

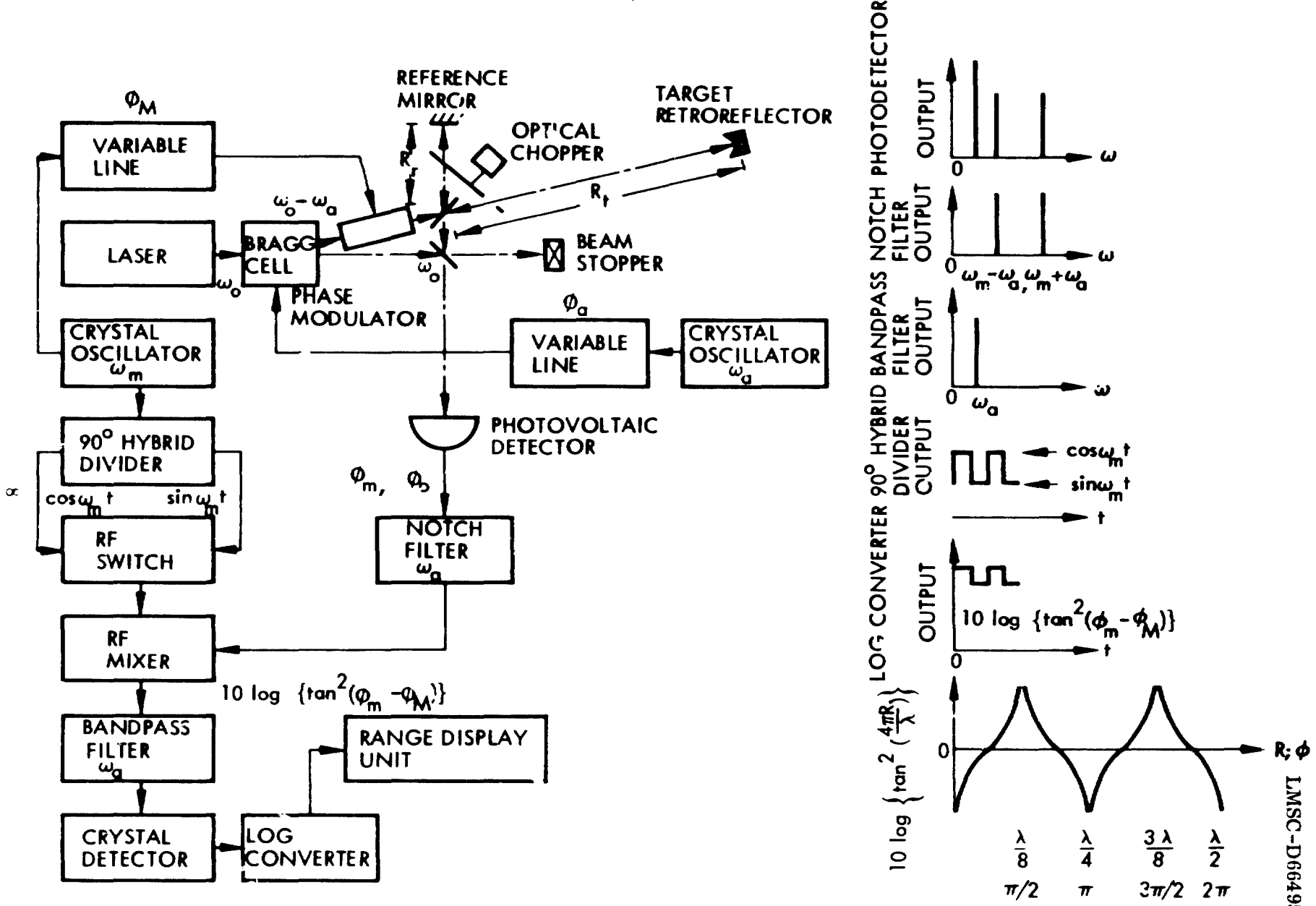


Fig. 2 Unique Signal Processing Flow Diagram with Illustrated Output Signal

$$\cos\left[(\omega_m + \omega_a)t - (\phi_o - \phi_a) + (\phi_m - \phi_M)\right] - \cos\left[(\omega_m - \omega_a)t + (\phi_o - \phi_a) + (\phi_m - \phi_M)\right] \quad (1)$$

where parameters are defined as

| | | |
|---|---|---|
| $\omega_m$ | = | angular frequency of phase modulation |
| $\omega_a$ | = | angular frequency of acoustic wave driving dual Bragg cell |
| $t$ | = | time |
| $\phi_o$ | = | range related optical phase = $4\pi R/\lambda_o$ |
| $R$ | = | range |
| $\lambda_o$ | = | optical wavelength |
| $\phi_m$ | = | range related modulation phase = $4\pi R/\lambda_m$ |
| $\lambda_m$ | = | modulation wavelength |
| $\phi_a$, $\phi_M$ | = | phase constants |

Suppose we mix these two sidebands (at frequencies $\omega_m + \omega_a$ amd $\omega_m - \omega_a$) with $\cos \omega_m t$ and $\sin \omega_m t$ alternately (which are derived from a 90-degree hybrid power divider) by using an RF mixer. Then the output of the RF mixer will contain $\sin(\phi_m - \phi_M) \sin(\omega_a t + \phi_o - \phi_a)$ and $\cos(\phi_m - \phi_M) \sin(\omega_a t + \phi_o - \phi_a)$, alternately. If we take the amplitude ratio of these two alternate signals, a range related function $\tan(\phi_m - \phi_M) = \tan(4\pi R/\lambda_m - \phi_M)$ will be obtained. Since we take the ratio of two RF mixer outputs to obtain range function, any variation of signal power, electronic gain, etc., is common to both outputs and are cancelled. The theoretical details on range function and range resolution derivations are described in the following subsection.

### 2.3.1 Principle of Operation

With a dual Bragg cell used, the laser output at frequency $\omega_o$ is frequency translated to $\omega_o - \omega_a$. The frequency-untranslated beam is employed as the optical local oscillator (LO). After passing through the phase modulator, the frequency-translated beam is directed alternately to the target and reference mirrors at ranges $R_t$ and $R_r$, respectively. An optical chopper may be employed to select alternately between the target and reference beams. Upon return, the distance-measuring beam is made congruent with the LO beam and photodetected. The output of the photodetector is amplified and sent through a notch filter centered at frequency $\omega_a$ before reaching the RF mixer.

A 90-degree hybrid power divider employs a portion of the output of the oscillator at $\omega_m$ and presents two signals with a 90-degree phase difference to a SPDT RF switch and in turn to an RF mixer. The inputs combined by the mixer form the signals $\sin(\phi_m - \phi_M) \sin(\omega_a t + \phi_o - \phi_a)$ and $\cos(\phi_m - \phi_M) \sin(\omega_a t + \phi_o - \phi_a)$ according to whether the RF switch is passing $\cos \omega_m t$ or $\sin \omega_m t$. The bandpass filter selects only those spectral components at frequency $\omega_a$. The output of a square law crystal detector thus consists of signals with amplitudes $\sin^2(\phi_m - \phi_M)$ or $\cos^2(\phi_m - \phi_M)$. By taking the logarithmic difference of these two signals we obtain:

$$10 \log \left[\sin^2(\phi_m - \phi_M)\right] - 10 \log \left[\cos^2(\phi_m - \phi_M)\right] = 10 \log \left[\tan^2(\phi_m(R) - \phi_M)\right]$$

The range, R, can be solved for explicitly in a simple, straightforward manner. The target range relative to the reference mirror can be calculated by subtracting two consecutive range measurements, one to the target and another to the reference mirror. A step-by-step analysis follows.

### 2.3.2 Range Function Derivation

With reference to Figure 2, the electric field at optical frequency $\omega_o - \omega_a$ of the return beam from a target at a range R can be expressed as

$$E_s = E_o \exp\left\{i\left[(\omega_o - \omega_a)t + (\phi_o - \phi_a) + \phi(t)\right]\right\} \quad (2)$$

where

| | | |
|---|---|---|
| $E_o$ | = | amplitude of electric field |
| $\phi_a$ | = | electronic phase angle related to cable length and variable line for RF signals at $\omega_a$ |
| $\phi(t)$ | = | $4\pi b/\lambda_o \sin(\omega_m t + \phi_m - \phi_M)$ |
| $4b/\lambda_o$ | = | modulation depth |
| $\phi_M$ | = | electronic phase angle related to cable length and variable line for RF signals at $\omega_m$. |

The electric field of the optical LO can be expressed as

$$E_L = E_\ell \exp\{i\omega_o t\} \quad (3)$$

where $E_\ell$ = amplitude of electric field.

The net laser radiation electric field on the photodetector is the sum of Equations (2) and (3) or

$$E = E_o \exp\left\{i\left[(\omega_o - \omega_a)t + (\phi_o - \phi_a) + A\sin(\omega_m t + \phi_m - \phi_M)\right]\right\} + E_\ell \exp\{i\omega_o t\} \quad (4)$$

where $A = 4\pi b/\lambda_o$.

Optical power received by the detector is proportional to the product of Equation (4) and its complex conjugate or

$$P \propto E\,E^* = E_o^2 + E_\ell^2 + 2E_o\,E_\ell \cos\left[(\omega_a t - \phi_o + \phi_a) - A \sin(\omega_m t + \phi_m - \phi_M)\right]$$

This can also be expressed as

$$P = P_o + P_\ell + 2\sqrt{P_o\,P_\ell}\cos\left[(\omega_a t - \phi_o + \phi_a) - A \sin(\omega_m t + \phi_m - \phi_M)\right]$$

$$= P_o + P_\ell + P_s$$

where

$P_o$ = DC component of signal power
$P_\ell$ = optical LO power.

$$P_s = 2\sqrt{P_o\,P_\ell}\cos\left[(\omega_a t - \phi_o + \phi_a) - A \sin(\omega_m t + \phi_m - \phi_M)\right] \qquad (5)$$

The AC component of photo current is

$$I_s = \frac{\eta q P_s}{h\nu}$$

$$= \frac{2\eta q\sqrt{P_o\,P_\ell}}{h\nu}\cos\left[(\omega_a t - \phi_o + \phi_a) - A \sin(\omega_m t + \phi_m - \phi_M)\right] \qquad (6)$$

Here we have used Equation (5), where

$\eta$ = quantum efficiency of the photodetector diode
$q$ = charge of electron
$h\nu$ = laser photon energy.

Equation (6) can also be expressed as a Fourier-Bessel expansion:

$$I_s = \frac{2\eta q \sqrt{P_o P_\ell}}{h\nu}\Big\{J_o(A)\cos(\omega_a t - \phi_o + \phi_a)$$

$$+ J_1(A)\Big[\cos(\omega_m t + \omega_a t - \phi_o + \phi_a + \phi_m - \phi_M)$$

$$- \cos(\omega_m t - \omega_a t + \phi_o - \phi_a + \phi_m - \phi_M)\Big]$$

$$+ J_2(A)\Big[\cos(2\omega_m t + \omega_a t - \phi_o + \phi_a + 2\phi_m - 2\phi_M)$$

$$-\cos(2\omega_m t - \omega_a t + \phi_o - \phi_a + 2\phi_m - 2\phi_M)\Big]$$

$$+ \ldots\ldots\Big\}$$

$$\approx \frac{2\eta q \sqrt{P_o P_\ell}}{h\nu}\cos(\omega_a t - \phi_o + \phi_a)$$

$$+ \frac{A\eta q \sqrt{P_o P_\ell}}{h\nu}\Big\{\cos\Big[(\omega_m + \omega_a)t - (\phi_o - \phi_a) + (\phi_m - \phi_M)\Big]$$

$$- \cos\Big[(\omega_m - \omega_a)t + (\phi_o - \phi_a) + (\phi_m - \phi_M)\Big]\Big\} \qquad (7)$$

For $A << 1$, the carrier is much stronger than the sidebands, and we have $J_o(A) \approx 1$, $J_1(A) \approx \frac{A}{2}$, $J_2(A) \approx 0$, etc. When the signal expressed by Equation (7) is mixed with a signal proportional to $\cos \omega_m t$, the result (output of the RF mixer) is

$$I_{S1} = K_{a1} I_s \cos \omega_m t$$

where $K_{a1}$ is a constant of proportionality. Substituting Equation (7) into the above equation yields

$$I_{S1} \approx \frac{K_{a1}\,\eta q\, P_o P_\ell}{h\nu}\left\{\cos\left[(\omega_m + \omega_a)t - \phi_o + \phi_a\right] + \cos\left[(\omega_m - \omega_a)t + \phi_o - \phi_a\right]\right\}$$

$$+ \frac{K_{a1} A \eta q \sqrt{P_o P_\ell}}{2h\nu}\left\{-2 \sin(\phi_m - \phi_M) \sin\left[\omega_a t - (\phi_o - \phi_a)\right]\right.$$

$$+ \cos\left[(2\omega_m + \omega_a)t - (\phi_o - \phi_a) + (\phi_m - \phi_M)\right]$$

$$\left. - \cos\left[(2\omega_m - \omega_a)t + (\phi_o - \phi_a) + (\phi_m - \phi_M)\right]\right\} \qquad (8)$$

The only term in Equation (8) that passes the bandpass filter is the term containing $\sin\left[\omega_a t - (\phi_o - \phi_a)\right]$. Therefore, the output of the bandpass filter is

$$i_{S1} = -\frac{t_a K_{a1} A \eta q \sqrt{P_o P_\ell}}{h\nu} \sin(\phi_m - \phi_M) \sin\left[\omega_a t - (\phi_o - \phi_a)\right] \qquad (9)$$

where $t_a$ is the transmission factor of the bandpass filter.

Similarly, taking signals from the mixer which mixes the signal current, $I_S$, with a signal proportional to $\sin \omega_m t$, the output of bandpass filter is

$$i_{S2} = -\frac{t_a K_{a2} A \eta q \sqrt{P_o P_\ell}}{h\nu} \cos(\phi_m - \phi_M) \sin\left[\omega_a t - (\phi_o - \phi_a)\right] \qquad (10)$$

The squares of Equations (9) and (10) represent a difference or "step" in output signal power. The square of the ratio of Equation (9) to Equation (10) "reflects" this signal difference or "step" at the output of the crystal detector, i.e.:

$$\frac{\overline{i_{S1}^2}}{\overline{i_{S2}^2}} = \left(\frac{K_{a1}}{K_{a2}}\right)^2 \tan^2(\phi_m - \phi_M) \qquad (11)$$

Taking the logarithm of both sides of Equation (11) gives

$$10 \log \left( \frac{\overline{i_{S1}^2}}{\overline{i_{S2}^2}} \right) = 10 \log \left[ \tan^2 \left( \frac{4\pi R}{\lambda_m} - \phi_M \right) \right] \qquad (12)$$

where we let $K_{a1} = K_{a2}$ for simplicity.

The lefthand side of Equation (12) represents power difference in the signal step (in dB); the right-hand side is an explicit function of range. The time sequence of signals comprising Equation (12) is illustrated in Figure 3.

The use of square-law detection assures that the output signal is positive. This in turn allows the use of logarithmic amplifier circuitry and yields an output signal step independent of variations in the returned laser beam power, $P_o$. However, it leaves the argument of $\tan^2$ in Equation (12) ambiguous and capable of falling in any of the four angle quadrants.

This ambiguity can be resolved in several ways. For example, let the first term of Equation (7) be isolated by a bandpass filter at frequency $\omega_a$ and then phase delayed by $\pi/2$. The resulting signal is proportional to $\sin \left[ \omega_a t - ( \phi_o - \phi_a ) \right]$ as are the signals of Equations (9) and (10). Thus if this signal is mixed with those of (9) and (10) the outputs are proportional to $-\sin ( \phi_m - \phi_M )$ and $-\cos ( \phi_m - \phi_M )$, respectively. Since the sine and cosine functions have unique pairs of algebraic signs in each of the four quadrants, the ambiguity of the $\tan^2$ function in Equation (12) can be resolved with the auxiliary circuitry suggested.

### 2.3.3 Range Resolution

Heterodyne detection is employed, and quantum noise is the dominant source of noise of the $CO_2$ system. The mean square signal at the output of the bandpass filter is

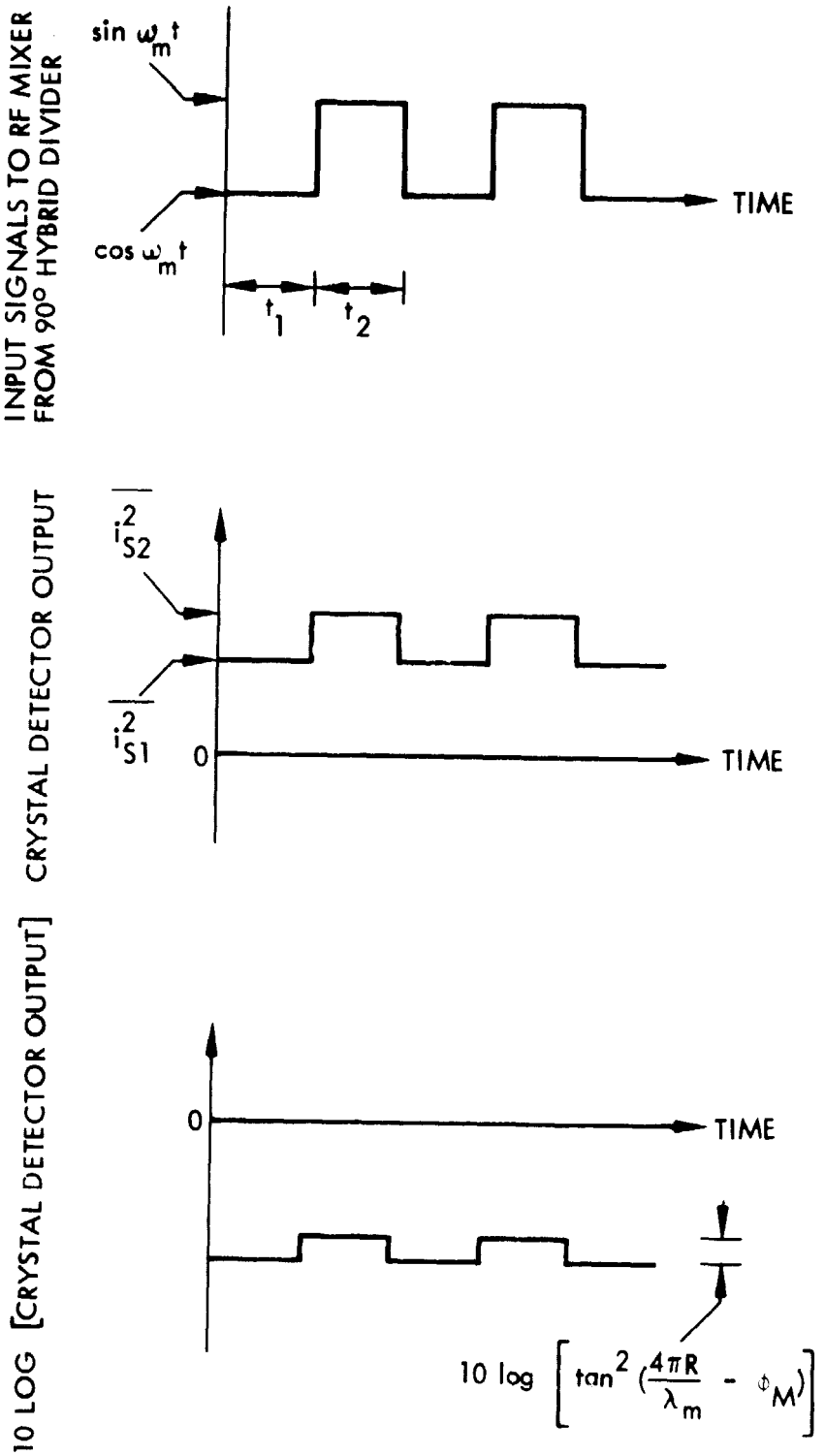


Fig. 3 Signal Time Sequence of Obtaining Range Function

$$i_{S1}^2 = \frac{t_a^2 K_{a1}^2 A^2 \eta^2 q^2 P_o P_\ell}{2h^2 \nu^2} \sin^2 (\phi_m - \phi_M) \qquad (13)$$

The mean-square quantum noise at the output of the bandpass filter is

$$i_{n1}^2 = \frac{2t_a^2 K_{a1}^2 q^2 \eta^2 B (P_o + P_\ell)}{h\nu}$$

$$\approx \frac{2t_a^2 K_{a1}^2 q^2 \eta B P_\ell}{h\nu} \qquad (14)$$

where $B$ is the electronic bandwidth and $P_\ell >> P_o$ is assumed.

During time period $t_1$ (Fig. 3), the statistical variation of signal current, $\Delta (i_{S1})_{rms}$, can be related to the uncertainty in phase, $(\Delta \phi_m)_1$, by

$$(i_{S1})_{rms} = - \sqrt{\frac{t_a^2 K_{a1}^2 A^2 \eta^2 q^2 P_o P_\ell}{2h^2 \nu^2}} (\Delta \phi_m)_1 \cos (\phi_m - \phi_M) \qquad (15)$$

Now, taking the square root of Equation (14) and setting it equal to Equation (15) and solving for $(\Delta \phi_m)$ yields the result:

$$(\Delta \phi_m)_1 = - \frac{2}{A\sqrt{\left(\frac{S}{N}\right) \cos (\phi_m - \phi_M)}}$$

where

$\left(\frac{S}{N}\right) = \frac{\eta P_o}{h\nu B}$ is the carrier signal-to-noise ratio.

Similarly, in the time period $t_2$, we have

$$(\Delta\phi_m)_2 = -\frac{2}{A\sqrt{\left(\frac{S}{N}\right)\sin(\phi_m - \phi_m)}}$$

Total resolvable phase angle is thus

$$\Delta\phi_m = \left|(\Delta\phi_m)_1\right| + \left|(\Delta\phi_m)_2\right|$$

$$= \frac{2}{A\sqrt{\left(\frac{S}{N}\right)}}\left[\frac{1}{|\cos(\phi_m - \phi_M)|} + \frac{1}{|\sin(\phi_m - \phi_M)|}\right]$$

which has a minimum value at $\phi_m - \phi_M = (2n+1)\frac{\pi}{4}$

where $n = 0, 1, 2, \ldots$ ; that is,

$$(\Delta\phi m)_{min} = \frac{4\sqrt{2}}{A\sqrt{\left(\frac{S}{N}\right)}} \qquad (16)$$

Since $\Delta\phi_m = \frac{4\pi}{\lambda m}\Delta R_m$ , the equation above can be related to minimum resolvable range, $(\Delta R_m)_{min}$ , here:

$$(\Delta R_m)_{min} = \frac{\lambda_m}{4\pi} (\Delta\phi_m)_{min}$$

$$= \frac{\lambda_m \sqrt{2}}{\pi A \sqrt{\left(\frac{S}{N}\right)}}$$

where $\lambda_m$ = modulation wavelength
$A$ = $\pi$ x (modulation depth)
$(S/N)$ = signal-to-noise ratio

$$\approx \frac{2 \left(\frac{\eta q}{h\nu}\right)^2 P_\ell P_s}{B \left(\frac{2q^2\eta}{h\nu} P_\ell + \frac{4kT_A}{R_L}\right)}$$

where

$\eta$ = detector quantum efficiency
$q$ = electron charge
$h\nu$ = photon energy
$P_\ell$ = optical local oscillator power
$P_s$ = optical signal power
$B$ = electronic bandwidth
$k$ = Boltzman's Constant
$T_A$ = equivalent temperature of amplifier
$R_L$ = resistance of load resistor

The range resolution of a HeNe SAS is found to be compatible with that for a $CO_2$ SAS for the typical parameters listed in Table 1:

Table 1

PARAMETERS FOR SAS RANGE RESOLUTION CALCULATION

| Parameters | HeNe System | $CO_2$ System |
|---|---|---|
| $\lambda_m$, meter | 3 | |
| Modulation Depth | 0.2 | 0.02 |
| $\eta$ | 0.8 | 0.5 |
| q, coul. | $1.6 \times 10^{-19}$ | |
| $h^{\nu}$, joul | $3.13 \times 10^{-19}$ | $1.87 \times 10^{-20}$ |
| $P_{\ell}$, watt | $10^{-3}$ | |
| $P_s$, watt | $10^{-6}$ | |
| B, $H_z$ | $10^{3}$ | |
| k, joul/$^oK$ | $1.38 \times 10^{-23}$ | |
| $T_A$, $^oK$ | * 596 | |
| $R_L$, ohm | 50 | |

*For an amplifier with 3 dB noise figure

which implies

$$\frac{(\Delta R_m)_{CO_2}}{(\Delta R_m)_{HeNe}} = \frac{160 \ \mu m}{104 \ \mu m} = 1.54$$

Range resolution can be improved by a factor $\sqrt{Bt}$ for a given integration time t and electronic bandwidth B. Subsequent to integration, the theoretically derived range resolution for a data rate of one reading per second is 10 $\mu$ m and 15 $\mu$ m for HeNe and $CO_2$ SAS, respectively. The digital integration process used employs a low duty cycle, hence the expected range resolution was somewhat degraded.

# 3.0 BREADBOARD IMPLEMENTATION

## 3.1 $CO_2$ LASER SYSTEM

The optical layout of the $CO_2$ system is shown in Figure 4. The two-color laser is not required for SAS, but was employed because the breadboard was also used for another system. The prisms were used only to recombine the two colors after they were separated by the Bragg cells. The electro-optic modulator was placed between Bragg cells No. 1 and No. 2, to minimize optical feedback to the laser. Bragg cell No. 3 is used only for optical isolation. The Bragg cells make good isolators because any return energy is frequency shifted and does not upset the laser.

## 3.2 HeNe LASER SYSTEM

The HeNe system optical layout is shown in Figure 5. Two scanning Bragg cells, one for transmitting the signal, the other for receiving signal, were driven synchronously for target/reference chopping. The target/reference chopping is hence achieved acoustooptically; mechanical chopping is thus avoided. The optical frequency shift caused by the transmitting scanning Bragg cell was restored by the receiving scanning Bragg cell and presented no problems to the signal processing electronics.

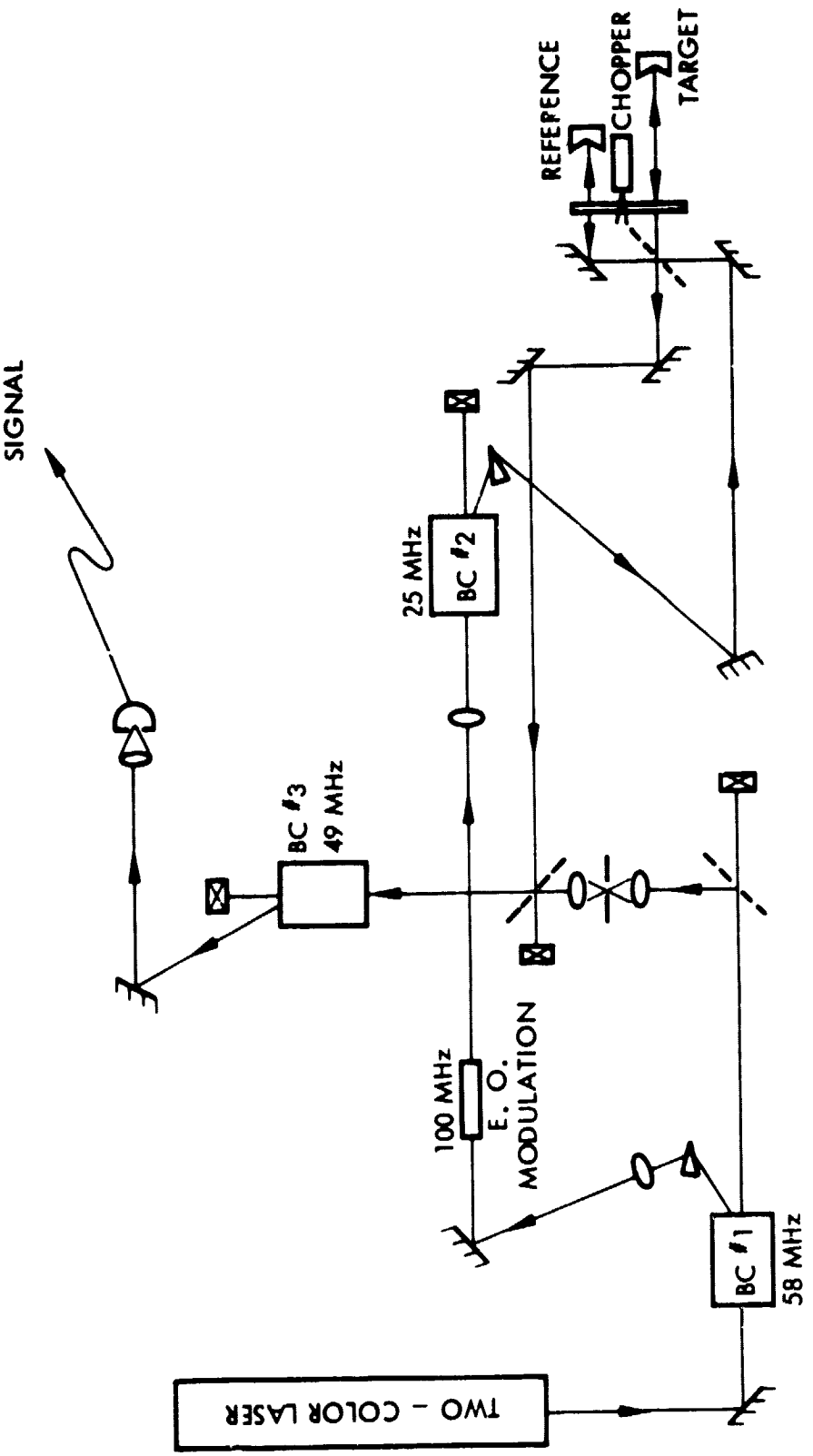


Fig. 4 $CO_2$ Optical Layout Diagram

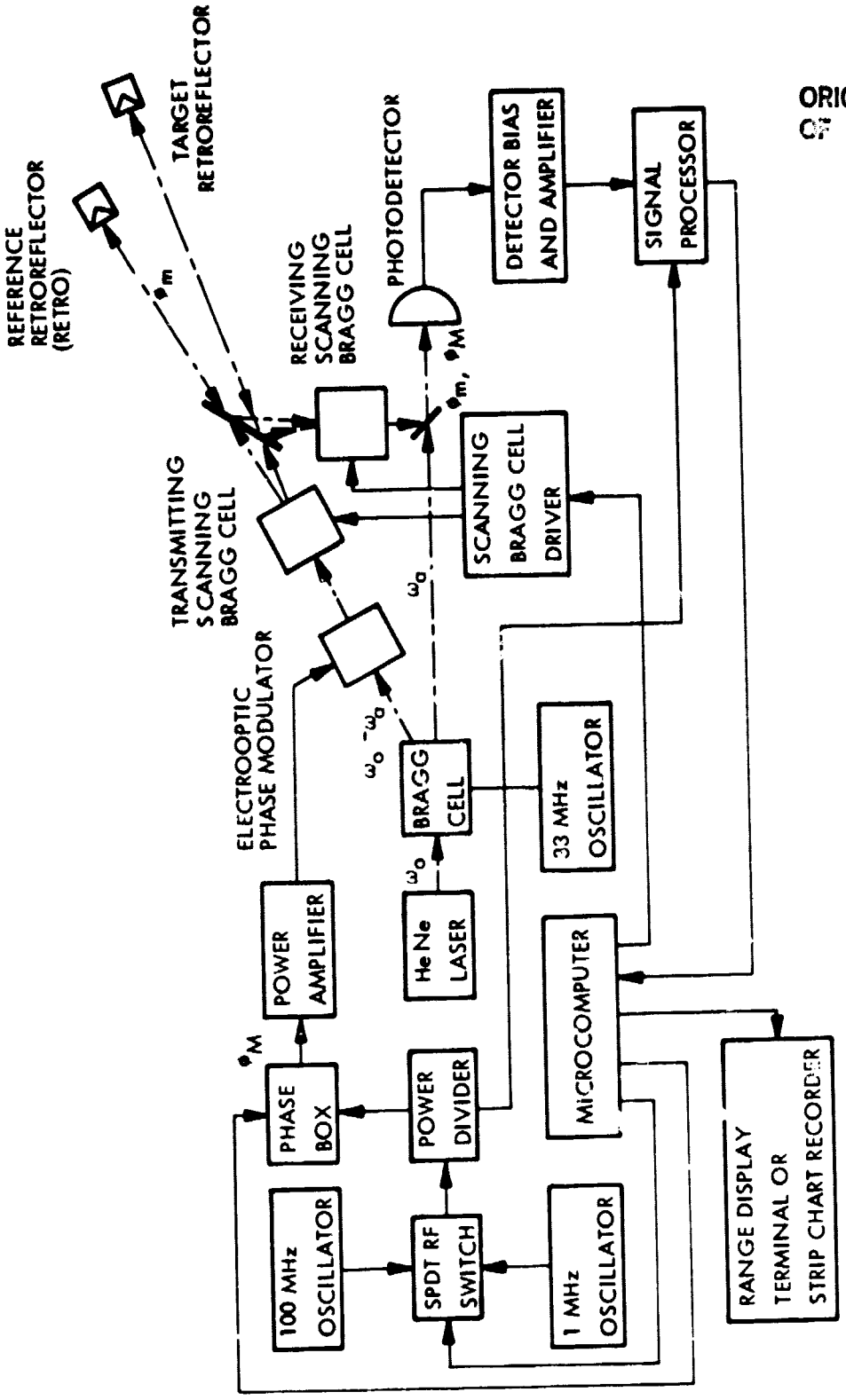


Fig. 5 HeNe SAS Layout Diagram

## 3.3 SIGNAL PROCESSING

A Cromemco Model Z-2D microcomputer was used to control the phase box, the rf switch, and the scanning Bragg cell driver, and was also used to integrate the range measurement for one second before the digital signal was converted into an analog signal for the strip chart recorder.

A digitized, range dependent function was presented by the signal processor to the microcomputer for data reduction and integration. For readout, the microcomputer digital output was also converted into an analog signal and displayed on a strip chart recorder.

For the laboratory tests a spectrum analyzer was used to provide the combination of bandpass filter, crystal detector, amplifier, and log converter. This output was digitized and then processed by the microcomputer. The 100 KHz bandwidth signal was switched at a rate of 360 Hz between target and reference. This signal was sampled eight times per step and the data averaged over approximately 1 second (displayed every 2 seconds). The data as presented by the strip chart recorder is shown in Section 4.

## 3.4 LABORATORY APPARATUS

Both the SAS breadboard systems are shown in the photograph of Figure 6. This shows the configuration of the $CO_2$ system as it existed when data was taken. The HeNe system was moved to the air suspension table prior to taking its data. This setup is shown in Figures 7 and 8 along with some of the $CO_2$ SAS breadboard components on the left in the photographs.

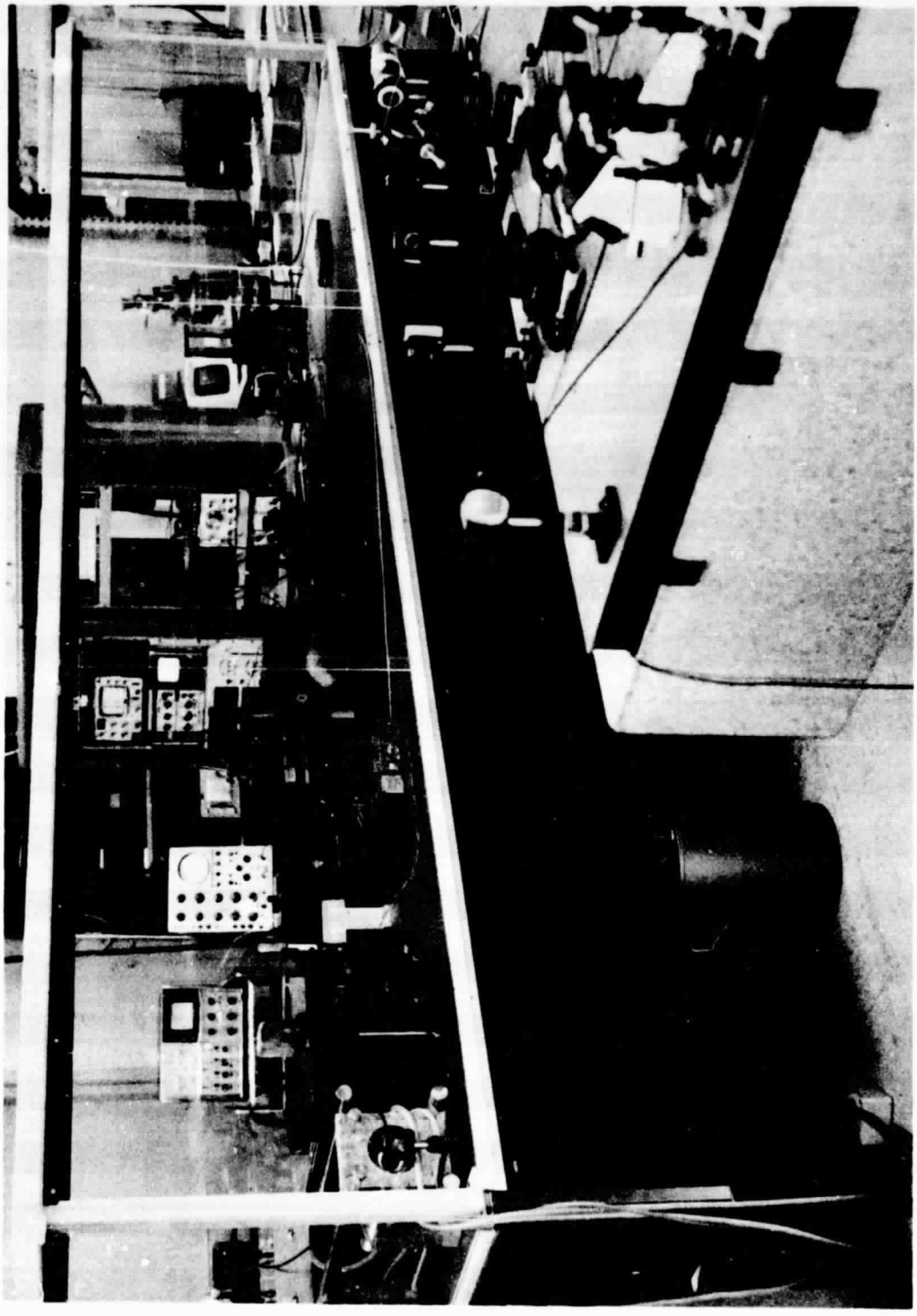

Fig. 6 SAS Breadboard Systems

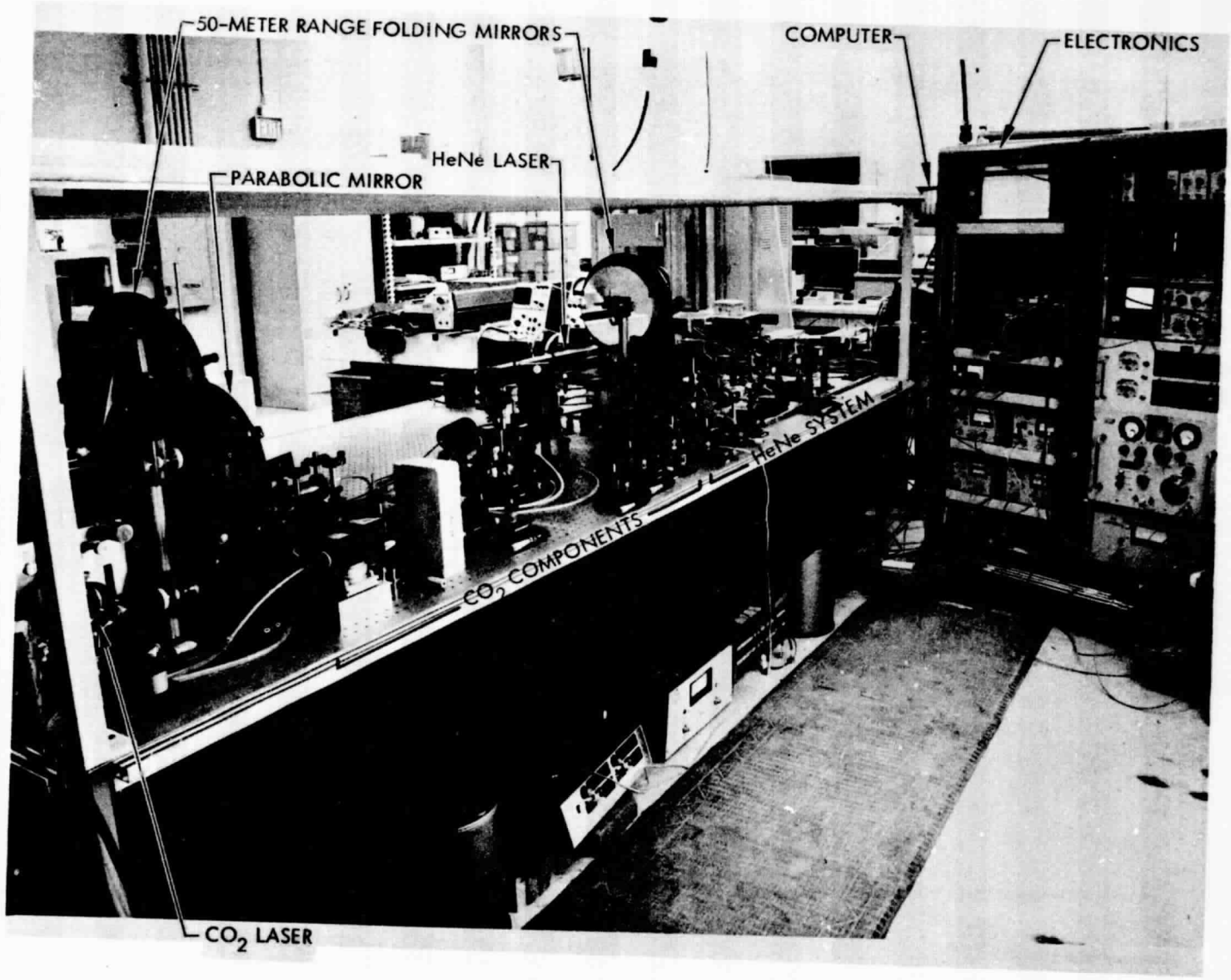


Fig. 7 HeNe SAS Breadboard System
(View 1)

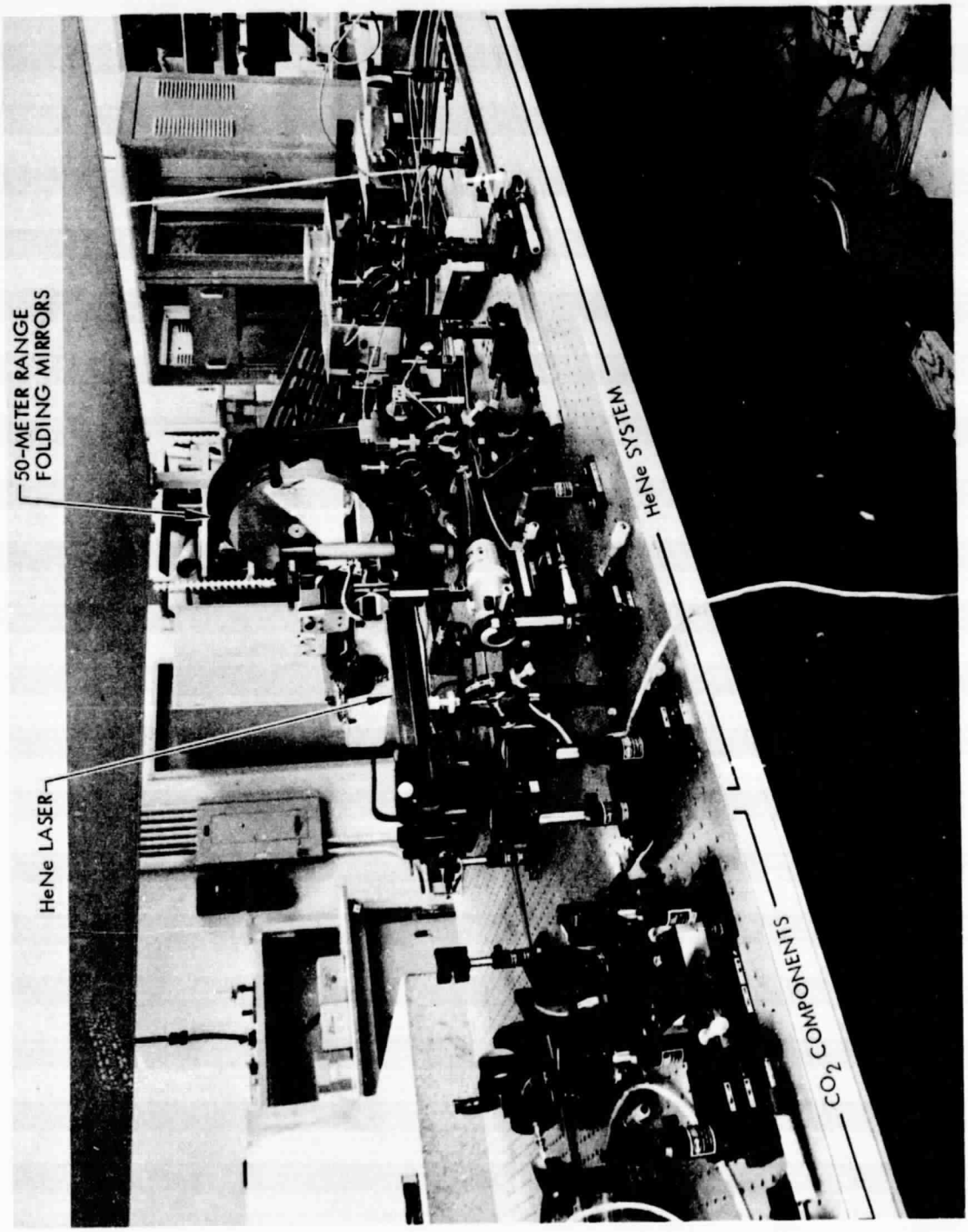


Fig. 8 HeNe SAS Breadboard System
(View 2)

# 4.0 TEST RESULTS

## 4.1 $CO_2$ LASER SYSTEM

The data from the $CO_2$ system measurements are shown in Figures 9 through 11. Resolution is demonstrated in Figure 9. The sensor alternately looked at the reference and target retros with the output (1 sec averages) plotted for about one minute. Then the target retro was moved 1 mm and that position held for a minute. This process was repeated twice. As can be seen, the data shows that an arbitrary measurement should repeat within 100 $\mu$m of any other measurement. Next, a linearity test was run to show how the logarithm remains linear when used near the $45^{o}$ point (Figure 10). The target was moved in steps of 0.05 inches over 1 inch. The 1 sec average data at each step (printed value) followed a straight line within 26 $\mu$m rms, ...pected noise error.

A long-term test was run and some drift noticed. This data is shown in Figure 11. The drift has been worse and seems to be a function of room thermal conditions and air movement. The problem is presently being worked on.

## 4.2 HeNe LASER SYSTEM

The resolution data for the HeNe System proved to be as good as the $CO_2$, except when switched from target to reference. The noise level increased by a factor of three when this was done, as shown in Figure 12. At this time, the source of this increased noise is unknown. It is either due to the laser instability or is possibly caused by optical feedback contamination. This problem will be resolved during LMSC'S 1979 ID program.

When the range was extended to 50m there was a significant increase in noise as shown in Figure 13. This was caused by the multi-reflection path used (a total of 44 reflections round trip) lowering the signal level too much. Observing the signal to

noise level on the spectrum analyzer indicated that direct correlation existed between loss in signal and increase in noise between the long path and short path measurements.

For a multi-target measurement, a parabolic reflector was used having the beam deflector at the center of curvature. (The parabola was very nearly a sphere). The sensor output was nearly constant over a set of eight points taken at several locations on the surface. The measurements, indicated a variation in curvature of about 1 mm over a 10 cm path across the mirror. Since the deviation was consistent in all the sets of data, and could not be an actual measurement of the mirror's deviation of curvature from that of a true spherical mirror, the only other possibility was that a consistent bias was being put in by the beam director. A 1 MHz modulator was not available, so an absolute distance measurement was not attempted.

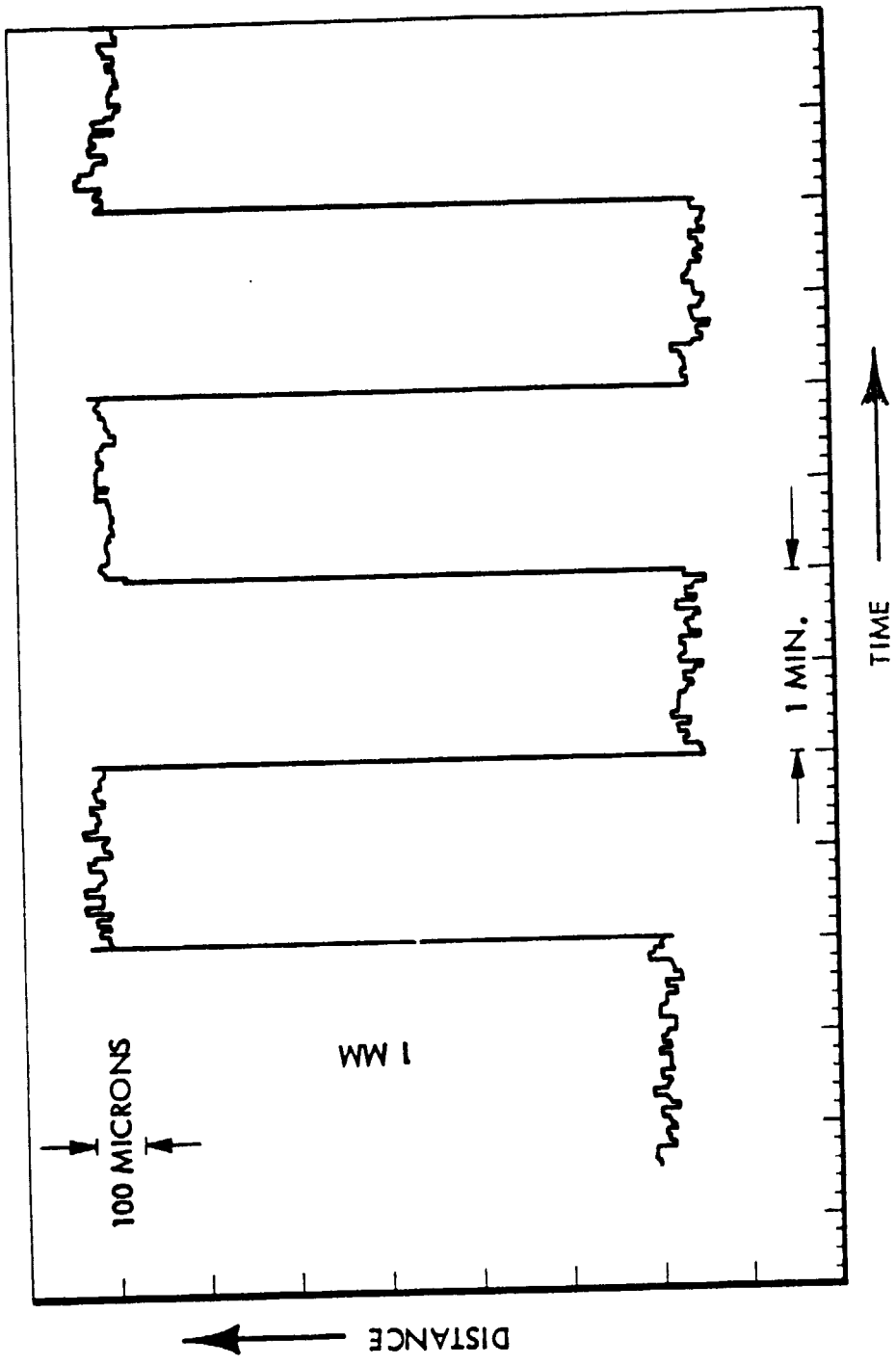


Figure 9 $CO_2$ SAS Range Resolution Data

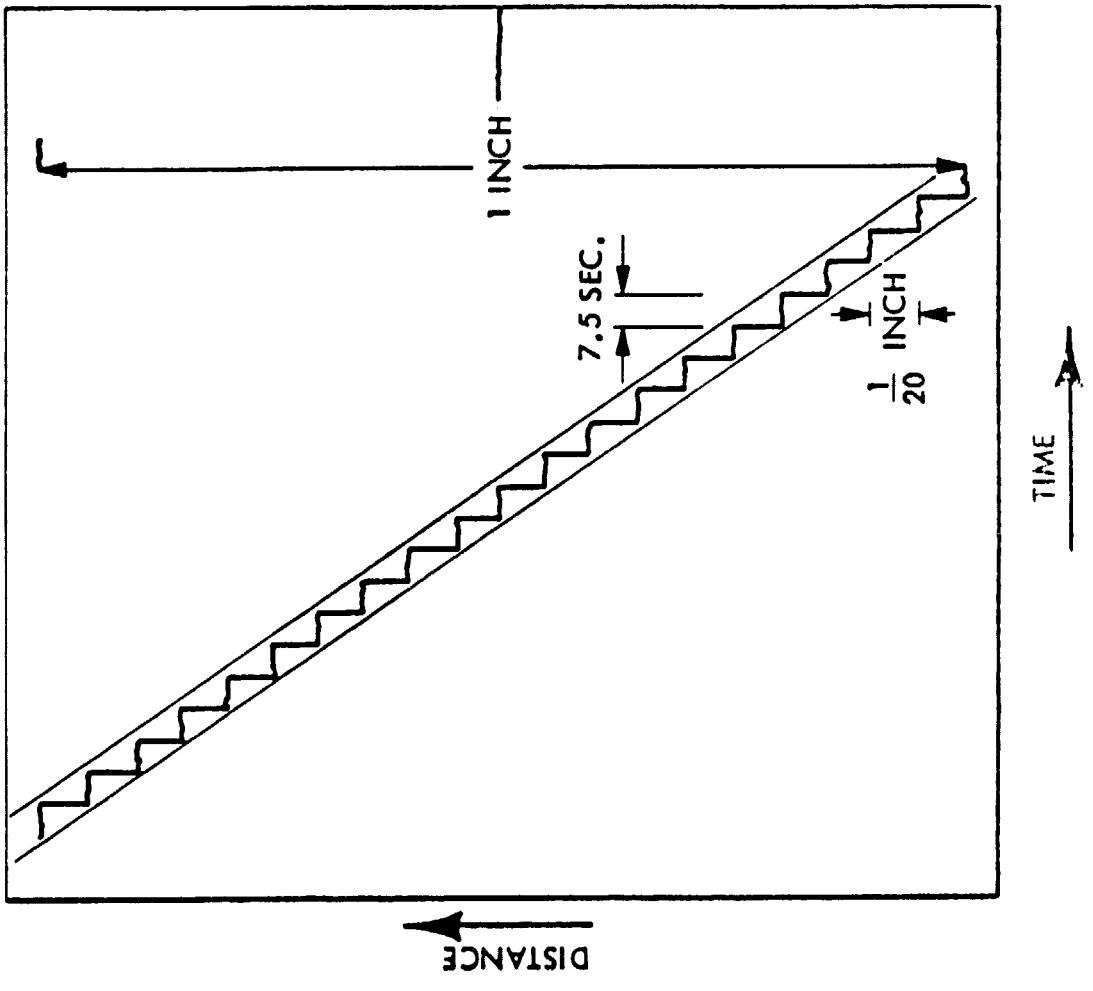


Figure 10 $CO_2$ SAS Range Measurement Linearity Data

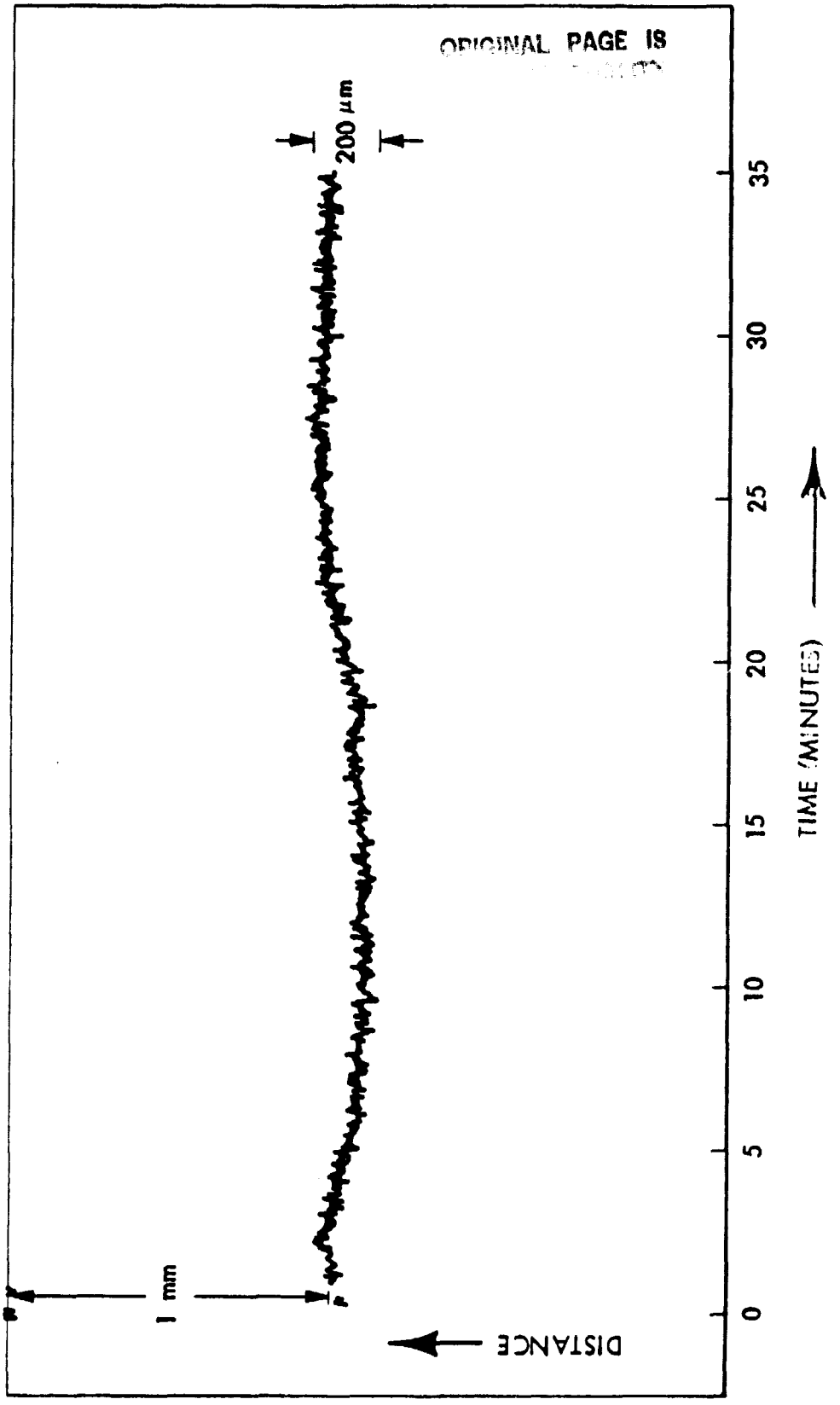


Figure 11. $CO_2$ SAS Range Measurement Drift Data

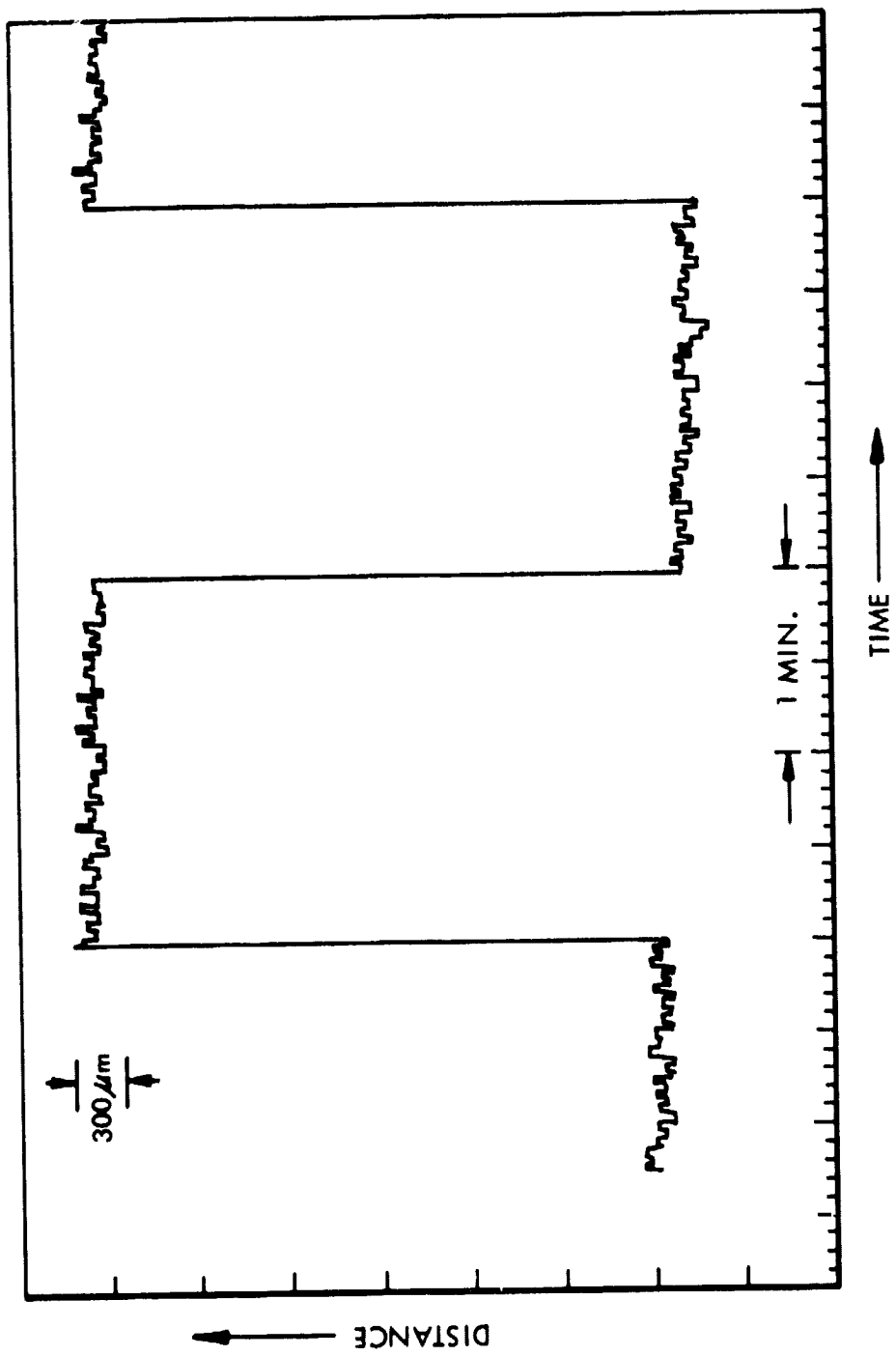


Figure 12. He Ne SAS Range Resolution Data

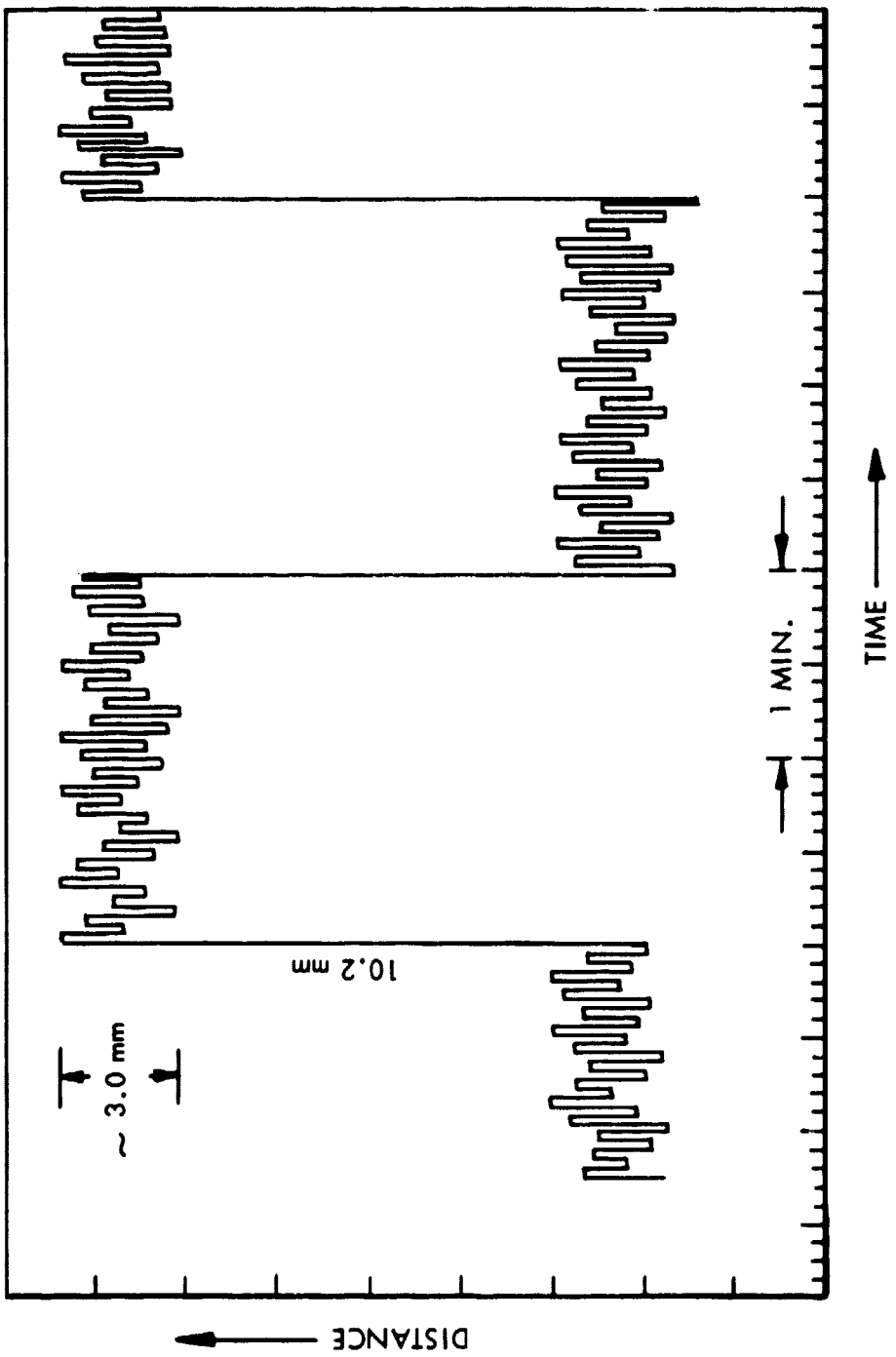


Figure 13. HeNe SAS 50-Meter Range Data

## 5.0 CONCLUSIONS

As a result of the test program conducted for this contract it is possible to state that nothing fundamental was discovered which would prevent the SAS from meeting its projected goals; however, some basic development is required before a system can be committed to design. LMSC plans to accomplish this development during 1979.

An SAS system could be designed using either a HeNe or $CO_2$ laser. The choice would be driven by requirements of bandwidth, signal strength, target characteristics, etc. If these allow the smaller, lower powered, less expensive HeNe system to be used, it should be used. It has the additional advantages of visual alignment and needing less development to qualify for space flight. The problems still needing to be worked on include 1) a stabilized single mode HeNe laser, 2) optical contamination and 3) skewing of the $CO_2$ laser beam. As mentioned previously, these are being addressed.

# 6.0 CONCEPTUAL SPACEFLIGHT SYSTEM

## 6.1 CONFIGURATION

A candidate deployment configuration for the SAS would be as illustrated in Figure 14. The SAS would be placed at the base of the antenna tower with a 2-axis beam director positioned out far enough to obtain a distance measurement which would reflect a meaningful change in contour (i.e., if the beam was only $30^{o}$ with respect to the rib there would be a 2 to 1 loss in sensitivity). Since the retro-reflectors will be in known positions on the ribs, only distance measurements are required to reconstruct the antenna figure. The retro-reflectors would be solid for HeNe or open for $CO_2$. The beam could be expanded to cover the expected spatial wander of the retro; no positional information would then be required for the beam director. It would be stepped to pre-programmed positions.

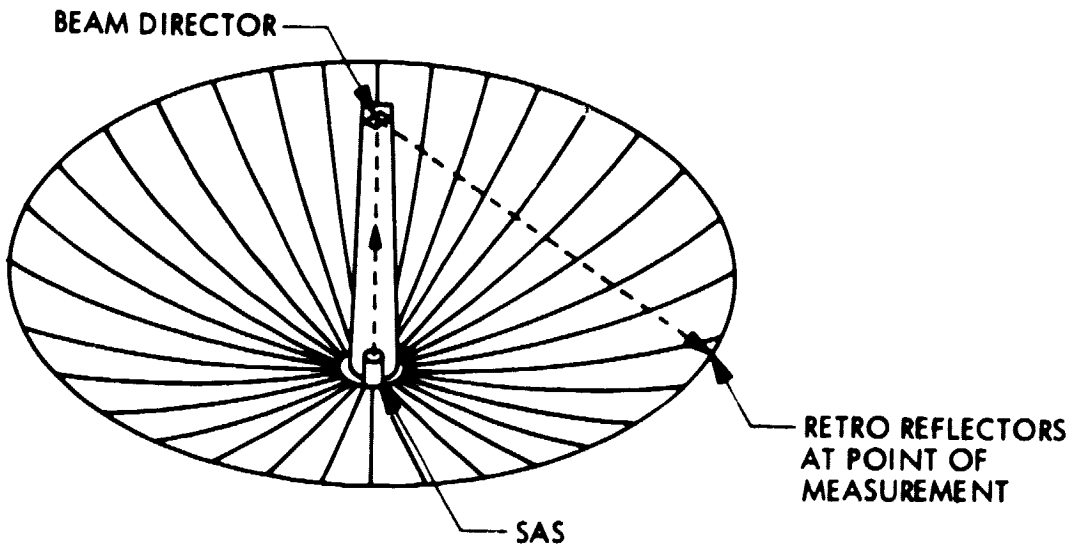


Figure 14 SAS Deployment

A 10 mw HeNe laser could be expanded to about 10 cm and still meet the basic accuracy requirements. If the retro wander cannot be contained within this value, either the $CO_2$ system or a hunting beam director to servo in on the target position would be required. If target angular position is necessary as part of an antenna measurement system, the beam director would require servopositioning and a position output signal.

## 6.2 SAS PACKAGING

Whether HeNe or $CO_2$, the SAS packaging configuration would be similar. The laser/optics/detector assembly would be placed as shown in Figure 14 with the signal processing and control electronics packaged separately. The electronics package would be similar for either system with the major share of the functions handled by a microprocessor. The $CO_2$ package would require considerable cooling capability for the laser and the cryogenic detector. Table 2 provides a comparison of the two systems estimated size, weight, and power. The cooling system requirements were not included since they would depend on the application environment.

Table 2

$CO_2$ VS. HeNe SAS TRADEOFF

| | Electro Optics | | | | |
|---|---|---|---|---|---|
| | HeNe | $CO_2$ | Electr. | Beam Director | Retro |
| Size (m) | 0.3 x 0.5 x 0.7 | 0.5 x 0.7 x 1.0 | 0.2 x 0.2 x 0.5 | 0.2 x 0.2 x 0.3 | $0.02^3$ |
| Weight (kg) | 7 | 20 | 2 | 2 | 0.02 |
| Power (w) | 300 | 800 | 10 | 3 | 0 |

## 6.3 MEASUREMENT TECHNIQUE TRADE-OFFS

To establish a baseline, prior to each set of measurements the beam director should be pointed back at the SAS; this will provide a calibration for the rest of the data. The analysis and test data indicate a peak-to-peak wander of less than 0.1 mm for a 1 sec integration. Since the noise is proportional to the square root of the integration time and the rms fluctuation is about one third the peak, an rms fluctuation of 0.1 mm would occur with a 0.1 sec integration time. Thus, the rate of measurement can be adjusted to the accuracy requirements.

The actual distance measured could be telemetered to the ground or a baseline could be established and stored on board with only deviations being telemetered, thus requiring less telemetry bandwidth. The number of positions monitored can be very large, limited only by the beam width and time available for measurement. Breadboard tests were run only with the 100 MHz modulator, providing an ambiguity distance of 0.75 m. If this is not sufficient for the test required, the 1 MHz modulation would be added to provide an ambiguity distance of 75 m. There is no fundamental reason why this could not be increased further if necessary. Tower movement would have to be accounted for by comparison of readings taken $180^{o}$ apart.

## 6.4 ESTIMATED PROGRAM COSTS

Based on the aforementioned system problems being resolved in 1979, the following development and production cost estimates have been made for the SAS with an accuracy of 0.1 mm and ambiguity distance of 75m, assuming a FY80 go ahead:

| | HeNe | | $CO_2$ | |
|---|---|---|---|---|
| | Estimated Cost | Months ARO | Cost | Months ARO |
| Design & Dev. (Thru Prototype) | $1.5 M | 18 | $2.0 M | 24 |
| Flight System (Space Shuttle) | $0.5 M | 24 | $0.7 M | 30 |

If the program reliability requirements would allow it, the prototype could be flown on an experimental flight. These costs are based on the present state of development and can be more accurately estimated as the 1979 ID program progresses. In addition, cooling system costs were not included, since these could very considerably be based on application.

DATE

FILMED

8 1979